Print ISSN : 0022-2755
Journal of Mines, Metals and Fuels
Contents available at: www.informaticsjournals.com/index.php/jmmf

Outcomes of Uniform as well as Non-Uniform Temperature Profiles on the Onset of Double Diffusive Magneto-Darcy-Rayleigh-Benard Convection in a two layer set up in the presence of Local Thermal Non-Equilibrium

R. Sumithra[1] and Shyamala Venkatraman[2*]

[1]Associate Professor and [2]Research Scholar, Department of UG, PG Studies & Research in Mathematics, Government Science College Autonomous, Nrupathunga University, Bengaluru, Karnataka, India sumitra_diya@yahoo.com and svr02009@gmail.com

Abstract :

Outcomes of uniform as well as non-uniform temperature profiles that is linear, parabolic, inverted parabolic, Piecewise Linear Profile Heated from Below (PLHB), Piecewise Linear Profile Cooled from Above (PLCA) and Step Function (SF) temperature profile on the onset of Double Diffusive Magneto-Darcy-Rayleigh-Benard (DDMDRB) Convection in a two layer set up in the presence of Local Thermal Non-Equilibrium with incompressible fluid horizontally surrounded by adiabatic rigid boundaries. Analytical solution to the attained problem is accomplished by means of regular perturbation technique. The consequences of altering the parameters namely fluid phase thermal expansion ratio, solid phase thermal expansion ratio, solid phase thermal diffusivity ratio, inter-phase diffusivity ratio, solute Rayleigh number, Chandrasekhar number, thermal ratio and porous parameter have been elucidated graphically.

Keywords: *Local Thermal Non Equilibrium (LTNE), Two Layer Set-up, Temperature Profiles, Regular Perturbation Technique*

Nomenclature:

English letters			
$\vec{q}_F = (u_F, v_F, w_F)$	: velocity vector	K	: permeability
t	: time	C_p	: specific heat capacity
P_F & P_P	: pressure	Q_F, Q_P	: Chandrasekhar numbers, defined below
g	: acceleration due to gravity	$\hat{S}$	: salinity ratio
T_F, T_{fP} & T_{sP}	: temperatures	C_0	: Interface species concentration
T_0	: interface temperature		

*Corresponding author

English letters			
h	: inter-phase heat transfer coefficient	R_F, R_{TfP}, R_{TsP}, R_{SF} & R_{SP}	: Rayleigh numbers, defined below
a_F & a_P	: non dimensional horizontal wave numbers	H	: scaled inter-phase heat transfer coefficient
n_F & n_P	: frequencies	$\hat{T}$	: thermal ratio
W_F & W_P	: dimensionless vertical velocities	$\hat{d}$	: depth ratio
Greek Symbols			
ρ_0	: referrence density	$\hat{\kappa}_{fp}$ & $\hat{\kappa}_{sP}$	: thermal diffusivity ratio
μ	: fluid viscosity	β	: porous parameter
ρ_F & ρ_P	: fluid density	β^2	: Darcy number
κ_F, κ_{fP} & κ_{sP}	: thermal diffusivities	τ	: inter-phase thermal diffusivity ratio
κ_{cF} & κ_{cP}	: solute diffusivities		
α_{TF}, α_{Tfp} & α_{TsP}	: thermal expansion coefficients	τ_{cF} & τ_{cP}	: solute diffusivity ratios
ϕ	: porosity	$\hat{\mu}$	: viscosity ratio
ζ_f & ζ_s	: thermal expansion ratio		
Subscripts			
P	: porous medium	S	: solid phase
f	: fluid phase	b	: basic state
F	: Fluid layer		

1. Introduction

Focus by researchers over problems on diffusion involving heat and concentration is tremendous because of its extensive significance in coupling of two fold blends, overspill of melt in soil of saturated nature, petroleum oil production, designing of solar pond, spinning technology etc. Such processes as exchange of heat, hydro-dissipation, precipitation of silver, crystallization of protein remarkably witness the role of magnetic field. Role of LTNE is significant in high speed flows with existence of larger temperature gradients between solid and fluid phases.

Daniel [1970] investigated the Global Stability of the thermosolutal Conduction-Diffusion Solution. Herbert [1984] studied the double-diffusive convection as a result of crystallization in magmas. Rudraiah & Malashetty [1986] examined the impact of coupled molecular diffusion on double-diffusive convection in a horizontal porous medium through linear and nonlinear stability analyses. Mulone [1994] analysed the nonlinear stability of a fluid layer of a mixture heated and salted from below. Atul & Bhadauria [2016] investigated the impact of magnetic field on fingering instability in a porous medium under cross-diffusion effect with respect to thermal non-equilibrium.

Altawallbeh et.al. [2018] investigated analytically the double-diffusive natural convection in a Maxwell fluid saturated porous layer in the presence of internal heat with respect to local thermal non-equilibrium model through linear stability analysis. Manjunatha & Sumithra [2018] studied the influence of non-uniform temperature gradients on surface tension driven two component magneto convection in a porous-fluid system. Xiaoli et.al. [2020] examined double diffusive magneto-hydrodynamic convective flows of a viscous fluid influenced by chemical reaction in the presence of heat source or sink under inclined magnetic field. Pulkit et.al. [2021] analysed double-diffusive convection in a rotating couple stress ferromagnetic fluid saturated porous medium

influenced by varying gravitational field and horizontal magnetic field. Safia et.al. [2021] investigated the effect of partial slip on the flow of Magneto- Carreau Nanofluid by double diffusive convection via inclined peristaltic asymmetric channel. Manjunatha et.al. [2021] examined the impact of nonuniform temperature gradients together with heat source on double diffusive Benard-Marangoni convection in a composite set up under vertical magnetic field. Ghazi et.al. [2022] studied the linear instability as well as nonlinear stability of Double-Diffusive Convection in a Rotating with LTNE Effects and Symmetric Properties: Brinkmann-Forchheimer Model.

Fragile investigations have been carried out on flow over composite layer influenced by LTNE. Enthused by the above survey of literatures, the present paper analyses the outcomes of uniform as well as non-uniform temperature profiles that is linear, parabolic, inverted parabolic, PLHB, PLCA and SF temperature profiles on the onset of Double Diffusive Magneto-Darcy-Rayleigh-Benard (DDMDRB) Convection in a two layer set up in the presence of Local Thermal Non-Equilibrium with incompressible fluid horizontally surrounded by adiabatic rigid boundaries.

2.0 Mathematical formulation

An infinite horizontal layer involving incompressible, Boussinesq electrically conducting fluid holding thickness $\mathbf{d_F}$ is considered. Densely packed porous layer saturated with same fluid with thickness $\mathbf{d_P}$ lies beneath the fluid layer levied with magnetic field of intensity H_0 in the perpendicular z-direction. The periphery below the porous layer as well as above the fluid layer are presumed to be rigid and free from surface tension effects based on temperature. A Cartesian coordinate system in which the origin is placed at the interface between fluid and porous layers and the z-axis pointing upright is considered. For the porous layer, solid phase as well as the fluid phase are purported to be in LTNE and a solid-fluid field model is considered to express distinctly the temperatures with regard to the solid and fluid phases. The Ordinary Differential Equations acquired from the governing equations, pertaining to the present research problem are

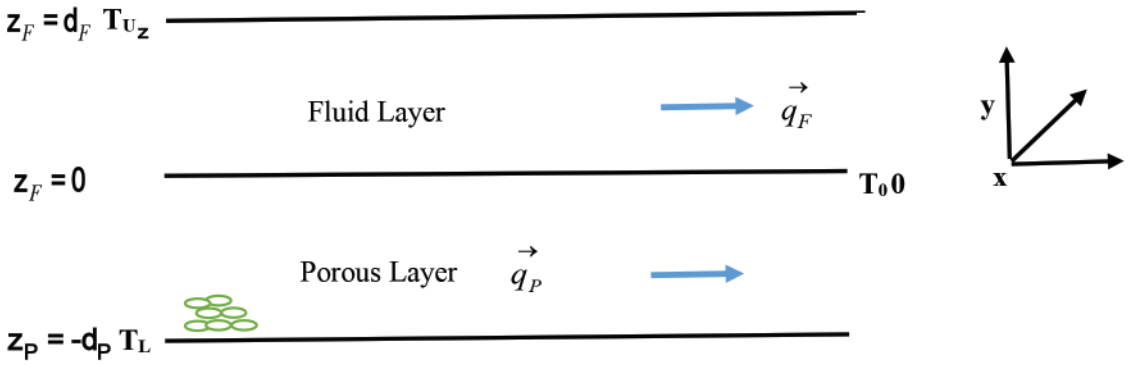

Figure 1: Outline of the Problem

In $\mathbf{0 \le z_F \le 1}$

$$(D^2 - a_F^{\,2})^2 W_F = R_F a_F^{\,2} \theta_F - R_{SF} a_F^{\,2} S_F + Q_F D^2 W_F \quad \text{... (1)}$$

$$(D^2 - a_F^{\,2}) \theta_F + W_F = 0 \quad \text{... (2)}$$

$$\tau_{cF} (D^2 - a_F^{\,2}) S_F + W_F = 0 \quad \text{... (3)}$$

In $\mathbf{0 \le z_P \le 1}$

$$(D_P^{\,2} - a_P^{\,2})^2 W_P = -\beta^2 R_{T_{fP}} a_P^{\,2} \theta_{fP} - \beta^2 R_{T_{sP}} a_P^{\,2} \theta_P \tau + \beta^2 R_{SP} a_P^{\,2} S_P \tau_{cP} - Q_P \beta^2 D_P^{\,2} W_P \quad \text{... (4)}$$

$$\phi (D_P^{\,2} - a_P^{\,2}) \theta_{fP} + W_P = -H(\theta_{sP} - \theta_{fP}) \quad \text{... (5)}$$

$$(1-\phi)(D_P^{\,2} - a_P^{\,2}) \theta_{sP} = H(\theta_{sP} - \theta_{fP}) \quad \text{... (6)}$$

$$\tau_{cP} (D_P^{\,2} - a_P^{\,2}) S_P + W_P = 0 \quad \text{... (7)}$$

For the fluid layer, $R_F = \frac{g\alpha_{TF}(T_0 - T_U)d_F^{\,3}}{\nu_1 \kappa_F}$ is the thermal Rayleigh number and $R_{SF} = \frac{g\alpha_{SF}(C_0 - C_U)d_F^{\,3}}{\nu_1 \kappa_F}$ is the solute Rayleigh number. For the porous layer, $R_{T_{fP}} = \frac{g\alpha_{T_{fP}}(T_L - T_0)d_P^{\,3}}{\nu_1 \kappa_{fP}}$ is the fluid phase Rayleigh number, $R_{T_{sP}} = \frac{g\alpha_{T_{sP}}(T_L - T_0)d_P^{\,3}}{\nu \kappa_{sP}}$ is the solid phase Rayleigh number, $R_{SP} = \frac{g\alpha_{SF}(T_L - T_0)d_P^{\,3}}{\nu \kappa_{sP}}$ is the solute Rayleigh number, $\beta^2 = \frac{K}{d_P^{\,2}} = Da$ represents Darcy number, $\tau = \frac{\kappa_{sP}}{\kappa_{fP}}$ represents ratio of thermal diffusivity of the solid phase to fluid phase, $\tau_{cF} = \frac{\kappa_{cF}}{\kappa_F}$ is the ratio of solute diffusivity to the thermal diffusivity in fluid layer, $\tau_{cP} = \frac{\kappa_{cP}}{\kappa_{fP}}$ is the ratio of solute diffusivity to the thermal diffusivity with respect to fluid in the porous layer, $H = \frac{h d_P^{\,2}}{\kappa_{fP}}$ is the scaled inter-phase heat transfer coefficient.

Equations (1) to (7) are ordinary differential equations of eighteenth order and required to be solved using the following boundary conditions.

3. Boundary conditions

Normal mode expansion performed on the appropriate boundary conditions after non dimensionalization. They are

$$W_F(1) = 0,\ DW_F(1) = 0,\ D\theta_F(1) = 0,\ DS_F(1) = 0,$$

$$\hat{T}W_F(0) = W_P(1),\ \hat{T}\hat{d}DW_F(0) = \hat{\mu}DW_P(1)$$

$$\theta_F(0) = \hat{T}\theta_{fP}(1),\ \theta_F(0) = \hat{T}\theta_{sP}(1),\ D\theta_F(0) = D\theta_{fP}(1),\ D\theta_F(0) = D\theta_{sP}(1)$$

$$S_F(0) = \hat{S}S_P(1),\ DS_F(0) = DS_P(1)$$

$$\hat{T}\hat{d}^3\beta^2[D^3W_F(0) - 3a_F^{\,2}DW_F(0)] = -DW_P(1) + \hat{\mu}\beta^2[D^3W_P(1) - 3a_P^{\,2}DW_P(1)]$$

$$\hat{T}\hat{d}^2(D^2 + a_F^{\,2})W_F(0) = \hat{\mu}(D^2 + a_P^{\,2})W_P(1)$$

$$W_P(0) = 0,\ DW_P(0) = 0,\ D\theta_{fP}(0) = 0,\ D\theta_{sP}(0) = 0,\ DS_P(0) = 0$$

Where $\hat{T} = \frac{T_L - T_0}{T_0 - T_U}$ is the thermal ratio, $\hat{S} = \frac{C_L - C_0}{C_0 - C_U}$ is the solute ratio, $\beta = \sqrt{\frac{K}{d_P^{\,2}}}$, $\hat{d} = \frac{d_P}{d_F}$ is the depth ratio and $\hat{\mu} = \frac{\mu_P}{\mu_F}$ is the viscosity ratio.

4. Solving using regular perturbation method

At boundaries with constant heat dissipation, convection occurs at smaller horizontal wave number 'a_F' . Hence we expand

$$\begin{bmatrix} W_F \\ \theta_F \\ S_F \end{bmatrix} = \sum_{j=0}^{\infty} a_F^{\,2j} \begin{bmatrix} W_{Fj} \\ \theta_{Fj} \\ S_{Fj} \end{bmatrix} \text{ and } \begin{bmatrix} W_P \\ \theta_{fP} \\ \theta_{sP} \\ S_P \end{bmatrix} = \sum_{j=0}^{\infty} a_P^{\,2j} \begin{bmatrix} W_{Pj} \\ \theta_{fPj} \\ \theta_{sPj} \\ S_{Pj} \end{bmatrix}$$

The solutions of zero order equations are obtained using an arbitrary factor and are

$W_{F0}(z_F)=0,\ \theta_{F0}(z_F)=\hat{T},\ W_{P0}(z_P)=0,\ \theta_{fP0}(z_P)=1,\ \theta_{sP0}(z_P)=1,\ S_{F0}(z_F)=\hat{S},\ S_{P0}(z_P)=1$

The first order equations in a_F^2 are:

For fluid layer,

$$D^4W_{F1}-Q_FD^2W_{F1}-R_F\hat{T}+R_{SF}\hat{S}=0 \quad \text{... (8)}$$

$$D^2\theta_{F1}-\hat{T}+W_{F1}=0 \quad \text{... (9)}$$

$$\tau_{cF}D^2S_{F1}-\tau_{cF}\hat{S}+W_{F1}=0 \quad \text{... (10)}$$

For porous layer,

$$D^2W_{P1}+Q_P\beta^2D^2W_{P1}+\beta^2R_{T_{fP}}+\beta^2R_{T_{sP}}\tau-\beta^2R_{SP}\tau_{cP}=0 \quad \text{... (11)}$$

$$(\phi D^2-H)\theta_{fP1}+H\theta_{sP1}+W_{P1}-\phi=0 \quad \text{... (12)}$$

$$[(1-\phi)D^2-H]\theta_{sP1}+H\theta_{fP1}-(1-\phi)=0 \quad \text{... (13)}$$

$$\tau_{cP}D^2S_{P1}-\tau_{cP}+W_{P1}=0 \quad \text{... (14)}$$

The corresponding boundary conditions are

$W_{F1}(1)=0,\ DW_{F1}(1)=0,\ D\theta_{F1}(1)=0,\ DS_{F1}(1)=0$

$\hat{T}W_{F1}(0)=\hat{d}^2W_{P1}(1),\ \hat{T}DW_{F1}(0)=\hat{\mu}\hat{d}DW_{P1}(1)$

$\theta_{F1}(0)=\hat{T}\hat{d}^2\theta_{fP1}(1),\ \theta_{F1}(0)=\hat{T}\hat{d}^2\theta_{sP1}(1)$

$D\theta_{F1}(0)=\hat{d}^2D\theta_{fP1}(1),\ D\theta_{F1}(0)=\hat{d}^2D\theta_{sP1}(1)$

$S_{F1}(0)=\hat{S}\hat{d}^2S_{P1}(1),\ DS_{F1}(0)=\hat{d}^2DS_{P1}(1)$

$\hat{T}\hat{d}\beta^2D^3W_{F1}(0)=-DW_{P1}(1)+\hat{\mu}\beta^2D^3W_{P1}(1),\ \hat{T}D^2W_{F1}(0)=\hat{\mu}D^2W_{P1}(1)$

$W_{P1}(0)=0,\ DW_{P1}(0)=0,\ D\theta_{fP1}(0)=0,\ D\theta_{sP1}(0)=0,\ DS_{P1}(0)=0$

W_{F1} and W_{P1} are obtained by solving equations (8) and (11) and are

$$W_{F1}(z_F)=B_1+B_2z_F+B_3\,\mathrm{Cosh}\left[\sqrt{Q_F}z_F\right]+B_4\,\mathrm{Sinh}\left[\sqrt{Q_F}z_F\right]-(R_F\hat{T}-R_{SF}\hat{S})\frac{z_F^{\,2}}{2Q_F} \quad \text{... (15)}$$

$$W_{P1}(z_P)=B_5+B_6z_P-\frac{\beta^2R_{T_{fP}}+\beta^2R_{T_{sP}}\tau-\beta^2R_{SP}\tau_{cP}}{2\left(1+Q_P\beta^2\right)}z_P^{\,2} \quad \text{... (16)}$$

Where the constants B_1, B_2, B_3, B_4, B_5 & B_6 evaluated using velocity boundary conditions are

$$B_1=A_1\left[A_2+\frac{\mathrm{Coth}\left[\sqrt{Q_F}\right]}{Q_F\sqrt{Q_F}}\left(\frac{1}{\hat{d}Q_F\sqrt{Q_F}}-A_2\right)-\frac{\mathrm{Sinh}\left[\sqrt{Q_F}\right]}{\hat{d}Q_F\sqrt{Q_F}}\right]+\frac{R_F\hat{T}-R_{SF}\hat{T}}{2Q_F}\left[1-\frac{2}{\sqrt{Q_F}\,\mathrm{Sinh}\left[\sqrt{Q_F}\right]}\right],$$

$$B_2=A_1\times A_2,\quad B_3=\frac{R_F\hat{T}-R_{SF}\hat{S}}{Q_F\sqrt{Q_F}\,\mathrm{Sinh}\sqrt{Q_F}}-\frac{A_1}{Q_F\sqrt{Q_F}\,\mathrm{Sinh}\sqrt{Q_F}}\left(\frac{1}{\hat{d}Q_F\sqrt{Q_F}}-A_2\right),\quad B_4=\frac{A_1}{\hat{d}Q_F\sqrt{Q_F}},$$

$$A_1=\frac{R_{SP}\tau_{cP}-R_{T_{fP}}-R_{T_{sP}}\tau)}{\hat{T}\left(1+Q_P\beta^2\right)},\ A_2=\frac{1}{\hat{d}Q_F}+\hat{\mu}\hat{d}\beta^2,\quad B_5=B_6=0$$

4.1. Solvability Condition:

The compatibility condition, derived by applying the corresponding boundary conditions to the differential equations with respect to heat and species concentration is

$$\int_0^1 W_{F1}(z_F) f(z_F) dz_F + \tau_{cP} \int_0^1 W_{F1}(z_F) dz_F + \hat{d}^2 \int_0^1 W_{P1}(z_P) g(z_P) dz_P + \hat{d}^2 \tau_{cF} \int_0^1 W_{P1}(z_P) dz_P = (\hat{d}^2 + \hat{T}) + (\hat{d}^2 + \hat{S}) \tau_{cF} \tau_{cP} \quad \text{... (17)}$$

4.2. Linear Temperature Profile:

For this profile, $f(z_F) = g(z_P) = 1$ ... (18)

For this model, the critical Rayleigh number is achieved by using (18) in (17) and is calculated as

$$R_{FC} = \frac{(\hat{d}^2 + \hat{T}) + (\hat{d}^2 + \hat{S}) \tau_{cF} \tau_{cP} + R_{SF} \left\{ \begin{array}{l} (1+\tau_{cP}) \left[\delta_{14} - \delta_{15} + \delta_{16} \right] - \hat{d}^4 \hat{\kappa}_{cP}{}^2 \tau_{cP} \times \\ \delta_1 \left[\delta_2 + \delta_3 + \delta_4 \times \delta_5 - \delta_6 - \delta_7 - \delta_8 \times \delta_5 + \delta_9 - \delta_{10} \right] \end{array} \right\}}{\begin{array}{l} (1+\tau_{cP}) \left[\delta_{14} - \delta_{15} + \delta_{16} \right] - \left[\zeta_f \hat{\kappa}_{fP}{}^2 + \zeta_s \hat{\kappa}_{sP}{}^2 \tau \right] \hat{d}^4 \times \\ \delta_1 \left[\delta_2 + \delta_3 + \delta_4 \times \delta_5 - \delta_6 - \delta_7 - \delta_8 \times \delta_5 + \delta_9 - \delta_{10} \right] \end{array}}$$

Where $\delta_1 = \frac{1+\tau_{cP}}{1+Q_P \beta^2}$, $\delta_2 = \frac{1}{\hat{d} Q_F \hat{T}}$, $\delta_3 = \frac{\hat{d} \hat{\mu} \beta^2}{\hat{T}}$, $\delta_4 = \frac{\text{Cosh}\sqrt{Q_F}}{\hat{T} Q_F \sqrt{Q_F}}$,

$$\delta_5 = \frac{1}{\hat{d} Q_F \sqrt{Q_F}} - \frac{1}{\hat{d} Q_F} - \hat{d} \hat{\mu} \beta^2$$

$$\delta_6 = \frac{\text{Sinh}\sqrt{Q_F}}{\hat{d} \hat{T} Q_F \sqrt{Q_F}}, \quad \delta_7 = \frac{1}{2\hat{T}} \left[\frac{1}{\hat{d} Q_F} - \hat{d} \hat{\mu} \beta^2 \right], \quad \delta_8 = \frac{1}{\hat{T} \sqrt{Q_F}}, \quad \delta_9 = \frac{\text{Cosh}\sqrt{Q_F}}{\hat{d} Q_F{}^2 \hat{T}} - \frac{1}{\hat{d} Q_F{}^2 \hat{T}},$$

$$\delta_{10} = \frac{\hat{d}(1+\tau_{cF}) \beta^2}{6(1+\tau_{cP})}, \quad \delta_{11} = \frac{\hat{T}}{2Q_F} \left(1 - \frac{2}{\sqrt{Q_F}\, \text{Sinh}\sqrt{Q_F}} \right), \quad \delta_{12} = \frac{\hat{T}}{Q_F{}^2}, \quad \delta_{13} = \frac{\hat{T}}{6Q_F},$$

$$\delta_{14} = \frac{\hat{S}}{2Q_F} \left(1 - \frac{2}{\sqrt{Q_F}\, \text{Sinh}\sqrt{Q_F}} \right), \quad \delta_{15} = \frac{\hat{S}}{Q_F{}^2}, \quad \delta_{16} = \frac{\hat{S}}{6Q_F}$$

and $\zeta_f = \frac{\alpha_{T_{fP}}}{\alpha_{TF}}$ represents ratio of the thermal expansion coefficients of fluid phase in porous layer to the thermal expansion coefficient with respect to fluid layer, $\zeta_s = \frac{\alpha_{T_{sP}}}{\alpha_{TF}}$ represents ratio of the thermal expansion coefficient of solid phase in porous layer to the thermal expansion coefficient in the fluid layer, $\hat{\kappa}_{fP} = \frac{\kappa}{\kappa_{fP}}$ represents ratio of thermal diffusivity in fluid layer to fluid phase thermal diffusivity in the porous layer, $\hat{\kappa}_{sP} = \frac{\kappa}{\kappa_{sP}}$ represents ratio of thermal diffusivity in fluid layer to solid phase thermal diffusivity in the porous layer, $\hat{\kappa}_{cP} = \frac{\kappa}{\kappa_{cP}}$ represents ratio of thermal diffusivity in fluid layer to solute diffusivity in the porous layer.

4.3. Parabolic Temperature Profile:

Here, $f(z_F) = 2z_F$ & $g(z_P) = 2z_P$ ... (19)

For this model, the critical Rayleigh number is achieved by using (19) in (17) and is calculated as

$$R_{FC}=\frac{(\hat{d}^2+\hat{T})+(\hat{d}^2+\hat{S})\tau_{cF}\tau_{cP}+R_{SF}\left\{\begin{matrix}\left(1+\tau_{cP}\right)\left[\Delta_{23}\Delta_{20}+\Delta_{24}\left(\Delta_{10}-\Delta_{11}+\Delta_{12}\right)-\Delta_{25}\right]-\\ \hat{d}^4\hat{\kappa}_{cP}{}^2\tau_{cP}\left[\begin{matrix}\Delta_1\left(\Delta_2+\Delta_3\Delta_4-\Delta_5\right)-\Delta_6\Delta_7-\\ \Delta_8\Delta_9\left(\Delta_{10}-\Delta_{11}+\Delta_{12}\right)+\Delta_{13}\left(\Delta_{14}-\Delta_{15}+\Delta_{16}\right)\end{matrix}\right]-\Delta_{17}\Delta_{18}\end{matrix}\right\}}{\begin{matrix}\Delta_{19}\Delta_{20}+\Delta_{21}\left(\Delta_{10}-\Delta_{11}+\Delta_{12}\right)-\Delta_{22}-[\zeta_f\hat{\kappa}_{fP}{}^2+\zeta_s\hat{\kappa}_{sP}{}^2\tau]\hat{d}^4\times\\ \left[\Delta_1\left(\Delta_2+\Delta_3\Delta_4-\Delta_5\right)-\Delta_6\Delta_7-\Delta_8\Delta_9\left(\Delta_{10}-\Delta_{11}+\Delta_{12}\right)+\Delta_{13}\left(\Delta_{14}-\Delta_{15}+\Delta_{16}\right)\right]-\Delta_{17}\Delta_{18}\end{matrix}}$$

Where $\Delta_1=\frac{1+\tau_{cP}}{\hat{T}\left(1+Q_P\beta^2\right)}$, $\Delta_2=\frac{1}{\hat{d}Q_F}+\hat{d}\hat{\mu}\beta^2$, $\Delta_3=\frac{-\mathrm{Co}t\,\mathrm{h}\sqrt{Q_F}}{Q_F\sqrt{Q_F}}$, $\Delta_4=\frac{-1}{\hat{d}Q_F\sqrt{Q_F}}+\frac{1}{\hat{d}Q_F}+\hat{d}\hat{\mu}\beta^2$,

$\Delta_5=\frac{-\mathrm{Sinh}\sqrt{Q_F}}{\hat{d}Q_F\sqrt{Q_F}}$, $\Delta_6=\frac{-1}{\hat{T}\left(1+Q_P\beta^2\right)}\left(\frac{2}{3}+\frac{1}{2}\tau_{cP}\right)$, $\Delta_7=\Delta_2$, $\Delta_8=\frac{1}{\hat{T}\left(1+Q_P\beta^2\right)Q_F\sqrt{Q_F}}$, $\Delta_9=\Delta_4$,

$\Delta_{10}=\frac{2\,\mathrm{Sinh}[\sqrt{Q_F}]}{\sqrt{Q_F}}$, $\Delta_{11}=\frac{2\left(\mathrm{Cosh}[\sqrt{Q_F}-1\right)}{Q_F}$, $\Delta_{12}=\frac{\tau_{cP}\,\mathrm{Sinh}[\sqrt{Q_F}]}{\sqrt{Q_F}}$, $\Delta_{13}=\frac{-1}{\hat{d}\hat{T}Q_F\sqrt{Q_F}\left(1+Q_P\beta^2\right)}$,

$\Delta_{14}=\frac{2\,\mathrm{Cosh}[\sqrt{Q_F}]}{\sqrt{Q_F}}$, $\Delta_{15}=\frac{2\,\mathrm{Sinh}[\sqrt{Q_F}]}{Q_F}$, $\Delta_{16}=\frac{\tau_{cP}\,\mathrm{Cosh}[\sqrt{Q_F}]}{\sqrt{Q_F}}$, $\Delta_{17}=\frac{-\hat{d}^2\beta^2}{1+Q_P\beta^2}$, $\Delta_{18}=\frac{1}{4}+\frac{1}{6}\tau_{cP}$,

$\Delta_{19}=\frac{\hat{T}}{2Q_F}$, $\Delta_{20}=1-\frac{2}{\sqrt{Q_F}\,\mathrm{Sinh}[\sqrt{Q_F}]}$, $\Delta_{21}=\frac{\hat{T}}{Q_F\sqrt{Q_F}\,\mathrm{Sinh}\sqrt{Q_F}}$, $\Delta_{22}=\frac{\hat{T}}{Q_F}\left(\frac{1}{4}+\frac{1}{6}\tau_{cP}\right)$,

$\Delta_{23}=\frac{\hat{S}}{2Q_F}$, $\Delta_{24}=\frac{\hat{S}}{Q_F\sqrt{Q_F}\,\mathrm{Sinh}\sqrt{Q_F}}$, $\Delta_{25}=\frac{\hat{S}}{Q_F}\left(\frac{1}{4}+\frac{1}{6}\tau_{cP}\right)$

And ζ_f, ζ_s, $\hat{\kappa}_{fP}$, $\hat{\kappa}_{sP}$, $\hat{\kappa}_{cP}$ remain the same as above.

4.4. Inverted Parabolic Temperature Profile:

Here, $f(z_F)=2(1-z_F)\ \&\ g(z_P)=2(1-z_P)$ ... (20)

For this model, the critical Rayleigh number is achieved by using (20) in (17) and is calculated as

$$R_{FC}=\frac{(\hat{d}^2+\hat{T})+(\hat{d}^2+\hat{S})\tau_{cF}\tau_{cP}+R_{SF}\left\{\begin{matrix}\left(1+\tau_{cP}\right)D_{18}D_{15}+D_9D_{19}-\hat{S}D_{17}-\hat{d}^4\hat{\kappa}_{cP}{}^2\tau_{cP}\\ \left[D_1\left(D_2+D_3\left(D_4-D_5\right)\right)-D_6D_7D_2-D_8D_9D_4+D_{10}D_{11}-D_{12}D_{13}\right]\end{matrix}\right\}}{\begin{matrix}\left(1+\tau_{cP}\right)D_{14}D_{15}+D_9D_{16}-\hat{T}D_{17}-[\zeta_f\hat{\kappa}_{fP}{}^2+\zeta_s\hat{\kappa}_{sP}{}^2\tau]\hat{d}^4\times\\ \left[D_1\left(D_2+D_3\left(D_4-D_5\right)\right)-D_6D_7D_2-D_8D_9D_4+D_{10}D_{11}-D_{12}D_{13}\right]\end{matrix}}$$

Where $D_1=\frac{1+\tau_{cP}}{\hat{T}\left(1+Q_P\beta^2\right)}$, $D_2=\frac{1}{\hat{d}Q_F}+\hat{d}\hat{\mu}\beta^2$, $D_3=\frac{-\mathrm{Co}t\,\mathrm{h}\sqrt{Q_F}}{Q_F\sqrt{Q_F}}$, $D_4=\frac{-1}{\hat{d}Q_F\sqrt{Q_F}}+\frac{1}{\hat{d}Q_F}+\hat{d}\hat{\mu}\beta^2$,

$D_5=\frac{\mathrm{Sinh}\sqrt{Q_F}}{\hat{d}Q_F\sqrt{Q_F}}$, $D_6=\frac{1}{3}+\frac{1}{2}\tau_{cP}$, $D_7=\frac{1}{\hat{T}\left(1+Q_P\beta^2\right)}$, $D_8=\frac{1}{\hat{T}\left(1+Q_P\beta^2\right)Q_F\sqrt{Q_F}\,\mathrm{Sinh}\left[\sqrt{Q_F}\right]}$,

$D_9=\frac{\tau_{cP}\,\mathrm{Sinh}[\sqrt{Q_F}]}{\sqrt{Q_F}}+\frac{2\left(\mathrm{Cosh}[\sqrt{Q_F}-1\right)}{Q_F}$, $D_{10}=\frac{1}{\hat{T}\hat{d}\left(1+Q_P\beta^2\right)Q_F\sqrt{Q_F}}$,

$$D_{11}=\frac{\tau_{cP}\,\mathrm{Cosh}[\sqrt{Q_F}\,]}{\sqrt{Q_F}}+\frac{2\,\mathrm{Sinh}[\sqrt{Q_F}}{Q_F},\ D_{12}=\frac{\hat{d}^2\beta^2}{1+Q_P\beta^2},\ D_{13}=\frac{1}{12}+\frac{1}{6}\tau_{cF},\ D_{14}=\frac{\hat{T}}{2Q_F},$$

$$D_{15}=1-\frac{2}{\sqrt{Q_F}\,\mathrm{Sinh}[\sqrt{Q_F}\,]},\ D_{16}=\frac{\hat{T}}{Q_F\sqrt{Q_F}\,\mathrm{Sinh}\sqrt{Q_F}},\ D_{17}=\frac{1}{Q_F}\left(\frac{7}{12}+\frac{1}{6}\tau_{cP}\right),\ D_{18}=\frac{\hat{S}}{2Q_F},$$

$$D_{19}=\frac{\hat{S}}{Q_F\sqrt{Q_F}\,\mathrm{Sinh}\sqrt{Q_F}}$$

And ζ_f, ζ_s, $\hat{\kappa}_{fP}$, $\hat{\kappa}_{sP}$, $\hat{\kappa}_{cP}$ remain the same as above.

4.5. Piecewise Linear Profile Heated from Below:

$$f(z_F)=\begin{cases}\varepsilon_F^{-1}, 0\le z_F\le\varepsilon_F\\ 0\quad ,\varepsilon_F\le z_F\le 1\end{cases}\text{ and }g(z_P)=\begin{cases}\varepsilon_P^{-1}, 0\le z_P\le\varepsilon_P\\ 0\quad ,\varepsilon_P\le z_P\le 1\end{cases}\qquad\text{... (21)}$$

For this model, the critical Rayleigh number is achieved by using (21) in (17) and is calculated as

$$R_{FC}=\frac{(\hat{d}^2+\hat{T})+(\hat{d}^2+\hat{S})\tau_{cF}\tau_{cP}+R_{SF}\left\{\begin{matrix}E_{20}E_{16}+E_{21}E_9-E_{22}-E_{23}-\hat{d}^4\hat{\kappa}_{cP}{}^2\tau_{cP}\\ \left[E_1\left(E_2+E_3E_4-E_5\right)-E_6E_7E_2-E_8E_4E_9+E_{10}E_{11}E_{12}-E_{13}E_{14}\right]\end{matrix}\right\}}{\begin{matrix}E_{15}E_{16}+E_{17}E_9-E_{18}E_{19}-[\zeta_f\hat{\kappa}_{fP}{}^2+\zeta_s\hat{\kappa}_{sP}{}^2\tau]\hat{d}^4\times\\ \left[E_1\left(E_2+E_3E_4-E_5\right)-E_6E_7E_2-E_8E_4E_9+E_{10}E_{11}E_{12}-E_{13}E_{14}\right]\end{matrix}}$$

Where $E_1=\frac{1+\tau_{cP}}{\hat{T}\left(1+Q_P\beta^2\right)}$, $E_2=\frac{-1}{\hat{d}Q_F}-\hat{d}\,\hat{\mu}\beta^2$, $E_3=\frac{-\mathrm{Co}t\,\mathrm{h}\sqrt{Q_F}}{Q_F\sqrt{Q_F}}$, $E_4=\frac{-1}{\hat{d}Q_F\sqrt{Q_F}}+\frac{1}{\hat{d}Q_F}+\hat{d}\,\hat{\mu}\beta^2$,

$$E_5=\frac{\mathrm{Sinh}\sqrt{Q_F}}{\hat{d}Q_F\sqrt{Q_F}},\ E_6=\frac{1}{\hat{T}\left(1+Q_P\beta^2\right)},E_7=\frac{\varepsilon}{2}+\frac{1}{2}\tau_{cP},\ E_8=\frac{1}{\hat{T}\left(1+Q_P\beta^2\right)Q_F\sqrt{Q_F}\,\mathrm{Sin}\,h\sqrt{Q_F}},$$

$$E_9=\frac{\tau_{cP}\,\mathrm{Sinh}[\sqrt{Q_F}\,]}{\sqrt{Q_F}}+\frac{\mathrm{Sinh}[\sqrt{Q_F}\varepsilon_F\,]}{\varepsilon_F\sqrt{Q_F}},\ E_{10}=\frac{-1}{1+Q_P\beta^2},E_{11}=\frac{-1}{\hat{T}\hat{d}Q_F\sqrt{Q_F}},$$

$$E_{12}=\frac{\mathrm{Cosh}[\sqrt{Q_F}\varepsilon_F\,]}{\varepsilon_F\sqrt{Q_F}}+\frac{\mathrm{Cosh}[\sqrt{Q_F}\,]\tau_{cP}}{\sqrt{Q_F}}-\frac{1}{\varepsilon_F\sqrt{Q_F}},\ E_{13}=\frac{-\hat{d}^2\beta^2}{6\left(1+Q_P\beta^2\right)},\ E_{14}=\varepsilon_P{}^2+\tau_{cF},\ E_{15}=\frac{\hat{T}}{2Q_F},$$

$$E_{16}=1-\frac{2}{\sqrt{Q_F}\,\mathrm{Sinh}[\sqrt{Q_F}\,]},\ E_{17}=\frac{\hat{T}}{Q_F\sqrt{Q_F}\,\mathrm{Sinh}\sqrt{Q_F}},\ E_{18}=\frac{\hat{T}}{6Q_F}\varepsilon_F{}^2,\ E_{19}=\frac{\hat{T}}{6Q_F}\tau_{cP},\ E_{20}=\frac{\hat{S}}{2Q_F},$$

$$E_{21}=\frac{\hat{S}}{Q_F\sqrt{Q_F}\,\mathrm{Sinh}\sqrt{Q_F}},\ E_{22}=\frac{\hat{S}}{6Q_F}\varepsilon_F{}^2,\ E_{23}=\frac{\hat{S}}{6Q_F}\tau_{cP}$$

And ζ_f, ζ_s, $\hat{\kappa}_{fP}$, $\hat{\kappa}_{sP}$, $\hat{\kappa}_{cP}$ remain the same as above.

4.6. Piecewise Linear Profile Cooled from Above:

In this case,

$$f(z_F)=\begin{cases}0\quad ,0\le z_F\le(1-\varepsilon_F)\\ \varepsilon_F^{-1},(1-\varepsilon_F)\le z_F\le 1\end{cases}\text{ and }\ g(z_P)=\begin{cases}0\quad ,0\le z_P\le(1-\varepsilon_P)\\ \varepsilon_P^{-1}\ ,(1-\varepsilon_P)\le z_P\le 1\end{cases}\qquad\text{... (22)}$$

For this model, the critical Rayleigh number is achieved by using (22) in (17) and is calculated as

$$R_{FC}=\frac{(\hat{d}^2+\hat{T})+(\hat{d}^2+\hat{S})\tau_{cF}\tau_{cP}+R_{SF}\left\{\begin{matrix}F_{21}F_{17}+F_{22}\left(F_9-F_{10}\right)-F_{23}-F_{24}-\hat{d}^4\hat{\kappa}_{cP}{}^2\tau_{cP}\\ \left[F_1\left(F_2+F_3F_4+F_5\right)+F_6F_7F_2-F_8F_4\left(F_9-F_{10}\right)+F_{11}\left(F_{12}-F_{13}\right)-F_{14}F_{15}\right]\end{matrix}\right\}}{\begin{matrix}F_{16}F_{17}+F_{18}\left(F_{19}-F_{20}\right)-F_9-F_{10}-[\zeta_f\hat{\kappa}_{fP}{}^2+\zeta_s\hat{\kappa}_{sP}{}^2\tau]\hat{d}^4\times\\ \left[F_1\left(F_2+F_3F_4+F_5\right)+F_6F_7F_2-F_8F_4\left(F_9-F_{10}\right)+F_{11}\left(F_{12}-F_{13}\right)-F_{14}F_{15}\right]\end{matrix}}$$

Where $F_1=\frac{1+\tau_{cP}}{\hat{T}\left(1+Q_P\beta^2\right)}$, $F_2=\frac{-1}{\hat{d}Q_F}-\hat{d}\hat{\mu}\beta^2$, $F_3=\frac{-\mathrm{Coth}\sqrt{Q_F}}{Q_F\sqrt{Q_F}}$, $F_4=\frac{-1}{\hat{d}Q_F\sqrt{Q_F}}+\frac{1}{\hat{d}Q_F}+\hat{d}\hat{\mu}\beta^2$,

$F_5=\frac{\mathrm{Sinh}\sqrt{Q_F}}{\hat{d}Q_F\sqrt{Q_F}}$, $F_6=\frac{1}{\hat{T}\left(1+Q_P\beta^2\right)}$, $F_7=\frac{1-\left(1-\varepsilon_F\right)^2}{2}+\frac{1}{2}\tau_{cP}$, $F_8=\frac{1}{\hat{T}\left(1+Q_P\beta^2\right)Q_F\sqrt{Q_F}\,\mathrm{Sin}h\sqrt{Q_F}}$,

$F_9=\frac{\tau_{cP}\,\mathrm{Sinh}[\sqrt{Q_F}]}{\sqrt{Q_F}}+\frac{\mathrm{Sinh}[\sqrt{Q_F}]}{\sqrt{Q_F}}$, $F_{10}=\frac{\mathrm{Sinh}[\sqrt{Q_F}(1-\varepsilon_F)]}{\sqrt{Q_F}}$, $F_{11}=\frac{-1}{\hat{T}\hat{d}Q_F\sqrt{Q_F}\left(1+Q_P\beta^2\right)}$,

$F_{12}=\frac{\mathrm{Cosh}[\sqrt{Q_F}]}{\sqrt{Q_F}}+\frac{\mathrm{Cosh}[\sqrt{Q_F}]\tau_{cP}}{\sqrt{Q_F}}$, $F_{13}=\frac{\mathrm{Cosh}[\sqrt{Q_F}\left(1-\varepsilon_F\right)]}{\sqrt{Q_F}}$, $F_{14}=\frac{-\hat{d}^2\beta^2}{6\left(1+Q_P\beta^2\right)}$,

$F_{15}=\frac{1-\left(1-\varepsilon_P\right)^3}{\varepsilon_P}+\tau_{cF}$, $F_{16}=\frac{\hat{T}}{2Q_F}$, $F_{17}=1-\frac{2}{\sqrt{Q_F}\,\mathrm{Sinh}[\sqrt{Q_F}]}$, $F_{18}=\frac{\hat{T}}{Q_F\sqrt{Q_F}\,\mathrm{Sinh}\sqrt{Q_F}}$,

$F_{19}=\frac{\hat{T}\tau_{cP}}{6Q_F}$, $F_{20}=\frac{\hat{T}}{6Q_F\varepsilon_F}\left[1-\left(1-\varepsilon_F\right)^3\right]$, $F_{21}=\frac{\hat{S}}{2Q_F}$,

$F_{22}=\frac{\hat{S}}{Q_F\sqrt{Q_F}\,\mathrm{Sinh}\sqrt{Q_F}}$, $F_{23}=\frac{\hat{S}\tau_{cP}}{6Q_F}$, $F_{24}=\frac{\hat{S}}{6Q_F\varepsilon_F}\left[1-\left(1-\varepsilon_F\right)^3\right]$

And ζ_f, ζ_s, $\hat{\kappa}_{fP}$, $\hat{\kappa}_{sP}$, $\hat{\kappa}_{cP}$ remain the same as above.

4.7. Step Function Temperature Profile:

In this profile, the basic temperature falls suddenly by an amount ΔT_F at $z_F=\varepsilon_F$ and ΔT_P at $z_p=\varepsilon_p$ otherwise uniform. Accordingly,

$$f(z_F)=\delta(z_F-\varepsilon_F)\,\&\,g(z_P)=\delta(z_P-\varepsilon_P) \quad \text{... (23)}$$

For this model, the critical Rayleigh number is achieved by using (23) in (17) and is calculated as

$$R_{FC}=\frac{(\hat{d}^2+\hat{T})+(\hat{d}^2+\hat{S})\tau_{cF}\tau_{cP}+R_{SF}\left\{\begin{matrix}G_{19}G_{15}+G_{20}G_{11}-G_{21}-G_{22}-\hat{d}^4\hat{\kappa}_{cP}{}^2\tau_{cP}\\ \left[G_1\left(G_2+G_3G_4-G_5\right)+G_6G_2G_8-G_9G_4G_{11}+G_{12}G_{13}+G_{23}G_{24}\right]\end{matrix}\right\}}{G_{14}G_{15}+G_{16}G_{11}-G_{17}-G_{18}-[\zeta_f\hat{\kappa}_{fP}{}^2+\zeta_s\hat{\kappa}_{sP}{}^2\tau]\hat{d}^4\times\left[G_1\left(G_2+G_3G_4-G_5\right)-G_6G_7G_8-G_9G_{10}G_{11}+G_{12}G_{13}+G_{23}G_{24}\right]}$$

Where $G_1=\frac{1+\tau_{cP}}{\hat{T}\left(1+Q_P\beta^2\right)}$, $G_2=\frac{-1}{\hat{d}Q_F}-\hat{d}\hat{\mu}\beta^2$, $G_3=\frac{-\mathrm{Coth}\sqrt{Q_F}}{Q_F\sqrt{Q_F}}$, $G_4=\frac{-1}{\hat{d}Q_F\sqrt{Q_F}}+\frac{1}{\hat{d}Q_F}+\hat{d}\hat{\mu}\beta^2$,

$G_5=\frac{\mathrm{Sinh}\sqrt{Q_F}}{\hat{d}Q_F\sqrt{Q_F}}$, $G_6=\varepsilon_F+\frac{1}{2}\tau_{cP}$, $G_8=\frac{1}{\hat{T}\left(1+Q_P\beta^2\right)}$, $G_9=\frac{1}{\hat{T}\left(1+Q_P\beta^2\right)Q_F\sqrt{Q_F}\,\mathrm{Sin}h\sqrt{Q_F}}$,

$$G_{11} = \frac{\tau_{cP}\,\mathrm{Sinh}[\sqrt{Q_F}]}{\sqrt{Q_F}} + \mathrm{Cosh}[\sqrt{Q_F}\,\varepsilon_F],\ G_{12} = \frac{-1}{\hat{T}\hat{d}Q_F\sqrt{Q_F}\left(1+Q_P\beta^2\right)},$$

$$G_{13} = \mathrm{Sinh}[\sqrt{Q_F}\,\varepsilon_F] + \frac{\mathrm{Cosh}[\sqrt{Q_F}]\tau_{cP}}{\sqrt{Q_F}},\ G_{14} = \frac{\hat{T}}{2Q_F},\ G_{15} = 1 - \frac{2}{\sqrt{Q_F}\,\mathrm{Sinh}[\sqrt{Q_F}]},\ G_{16} = \frac{\hat{T}}{Q_F\sqrt{Q_F}\,\mathrm{Sinh}\sqrt{Q_F}}$$

$$G_{17} = \frac{\hat{T}\tau_{cP}}{6Q_F},\ G_{18} = \frac{\hat{T}\varepsilon_F{}^2}{2Q_F},\ G_{19} = \frac{\hat{S}}{2Q_F},\ G_{20} = \frac{\hat{S}}{Q_F\sqrt{Q_F}\,\mathrm{Sinh}\sqrt{Q_F}},\ G_{21} = \frac{\hat{S}\tau_{cP}}{6Q_F},\ G_{22} = \frac{\hat{S}\varepsilon_F{}^2}{2Q_F},$$

$$G_{23} = \frac{-\hat{d}^2\beta^2}{6\left(1+Q_P\beta^2\right)},\ G_{24} = 3\varepsilon_P{}^2 + \tau_{cF}$$

And ζ_f, ζ_s, $\hat{\kappa}_{fP}$, $\hat{\kappa}_{sP}$, $\hat{\kappa}_{cP}$ remain the same as above.

5. Results and Discussions

Outcomes of uniform as well as non-uniform temperature profiles viz. linear, parabolic, inverted parabolic, PLHB, PLCA and SF temperature profile on the onset of DDMDRB convection are analysed with respect to LTNE model.

Graphical interpretation for critical Rayleigh number R_C versus depth ratio $\hat{d}$ for the fixed values of $\beta = 0.01$, $\zeta_f = 1$, $\zeta_s = 2$, $\hat{\kappa}_{sP} = 0.5$, $\tau = 0.1$, $Q_F = 5$, $R_{SF} = 5$ and $\hat{T} = 1$ has been performed with regard to linear, parabolic, inverted parabolic, PLHB, PLCA and SF thermal gradients in case of rigid boundaries. The stability of the profiles shows an interesting behaviour. For $0 < \hat{d} < 0.6$, PLHB is most unstable whereas for $\hat{d} > 0.6$, linear profiles is the most unstable one. Similarly, when $0 < \hat{d} < 0.9$, inverted parabolic profile is most stable and when $\hat{d} > 0.9$, PLCA takes the place.

The result on varying each of the variables namely porous parameter β, fluid phasse thermal expansion ratio ζ_f, solid phase thermal expansion ratio ζ_s, solid phase thermal diffusivity ratio $\hat{\kappa}_{sP}$, inter-phase diffusivity ratio τ, Chandrasekhar number Q_F, Solute Rayleigh number R_{SF} and thermal ratio $\hat{T}$ on critical Rayleigh number keeping the remaining parameters fixed are depicted with regard to both LTNE conditions via figures (3.1), (4.1), (5.1), (6.1), (7.1), (8.1) and (9.1) respectively for linear, parabolic and inverted parabolic temperatuer profile and via figures (3.2), (4.2), (5.2), (6.2), (7.2), (8.2), and (9.2) respectively for piecewise linear profile heated from below, piecewise linear profile cooled from above and step function temperature profile.

The effects of β, porous parameter on the critical Rayleigh number are shown in figures 3.1 and 3.2 It is seen that the curves are diverging with assigned

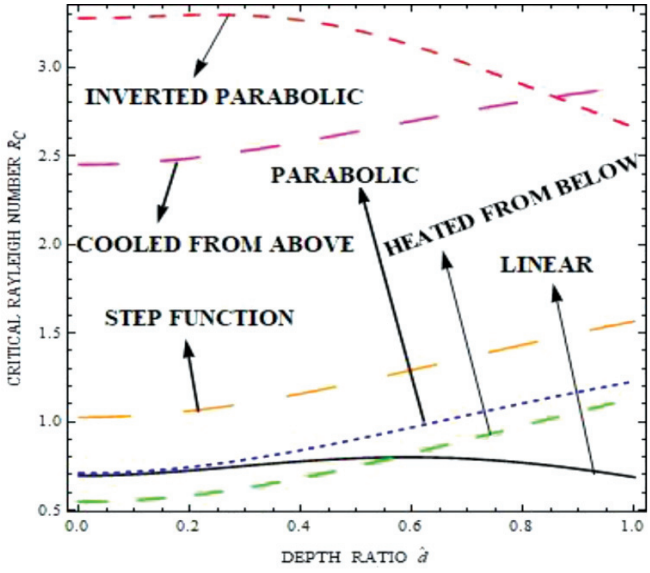

Figure-2: Comparison-Critical Rayleigh Number (RC) for 6 profiles with respect to LTNE model

values $\beta = 0.01$, 0.7 and 1 which proves that variation effect is protruding in case of two layer set up with $d \ll d_P$. It is also evident from the figure that increase in β results into decrease in critical Rayleigh number and hence the set-up can be destabilized resulting in earlier onset of DDMDRB convection. Surprisingly, exceptional case is observed in case of SF profile. SF profile postpones the onset of DDMDRB convection for more permeable medium. Also, it is observed from the graph that inverted parablic profile is most stable whereas the linear profile is most unstable. Similarly, PLCA is most stable whereas PLHB is most unstable. The effect of the parameter is very less for linear profile and higher for inverted parabolic profile the whereas the effect of the parameter is very less in case

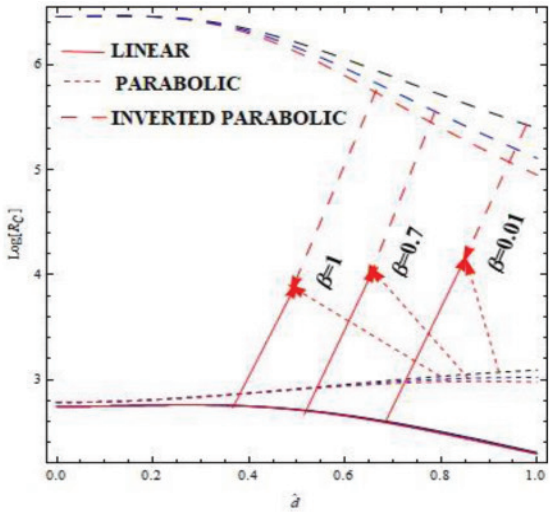

Figure 3.1

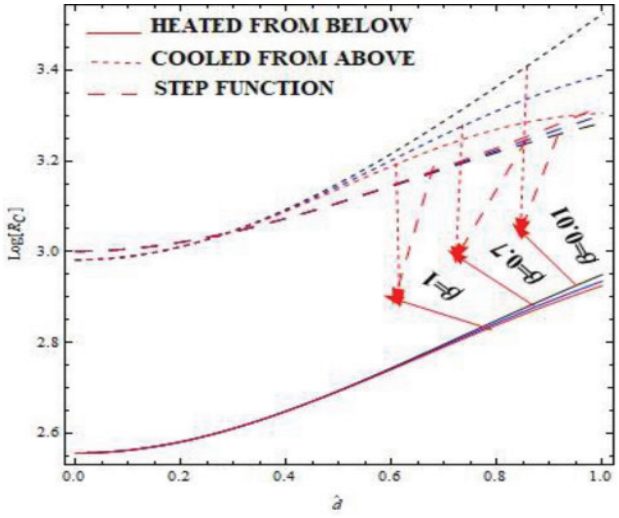

Figure 3.2

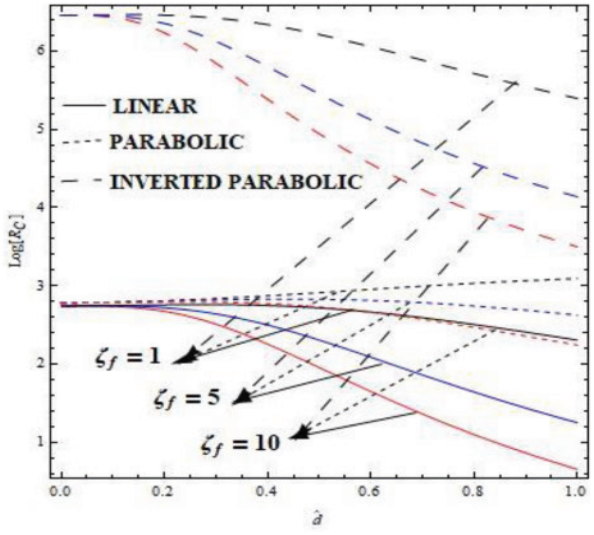

Figure 4.1

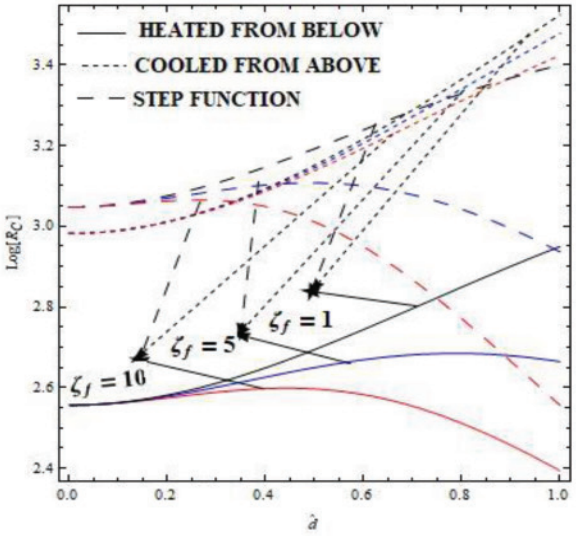

Figure 4.2

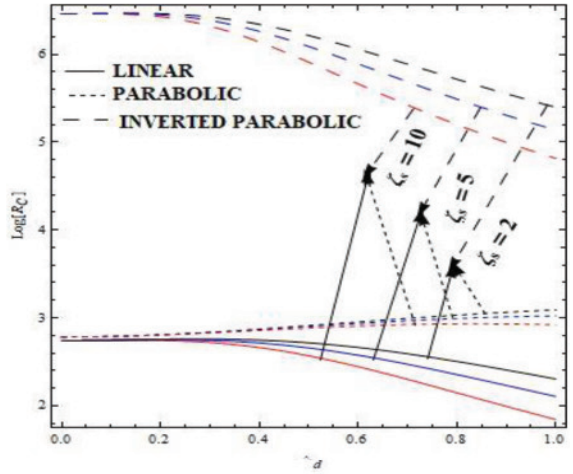

Figure 5.1

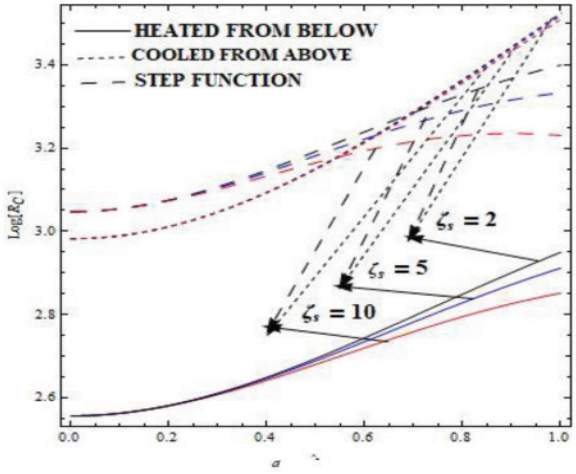

Figure 5.2

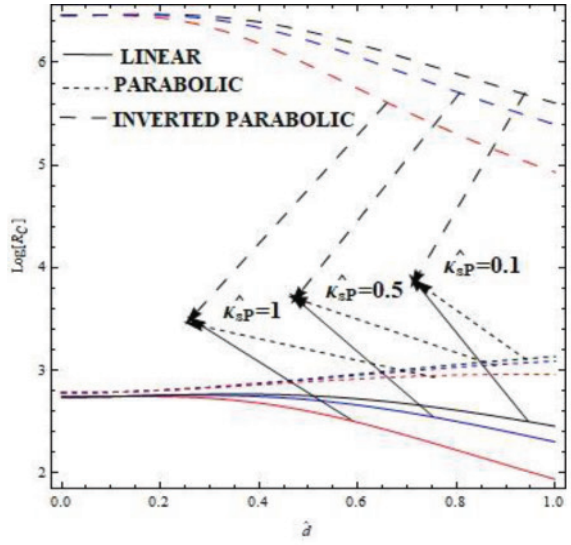

Figure 6.1

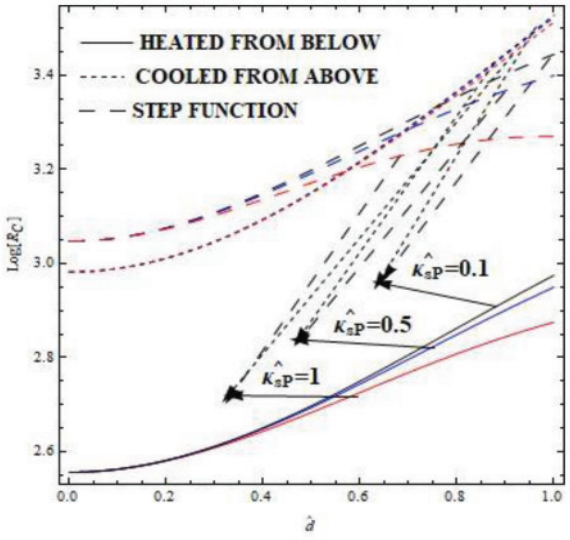

Figure 6.2

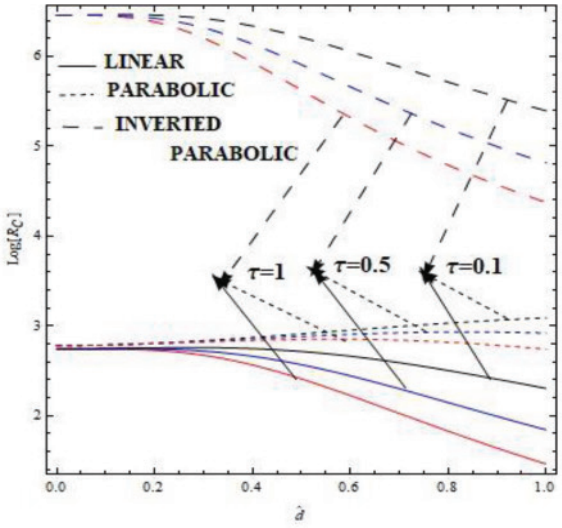

Figure 7.1

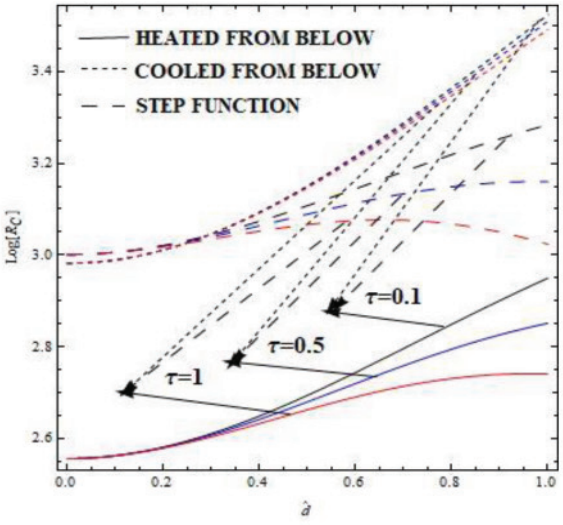

Figure 7.2

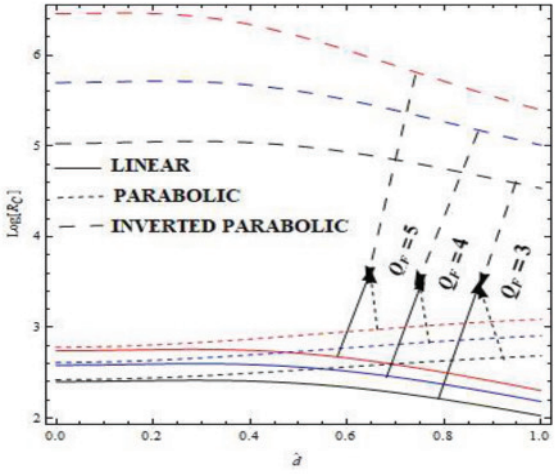

Figure 8.1

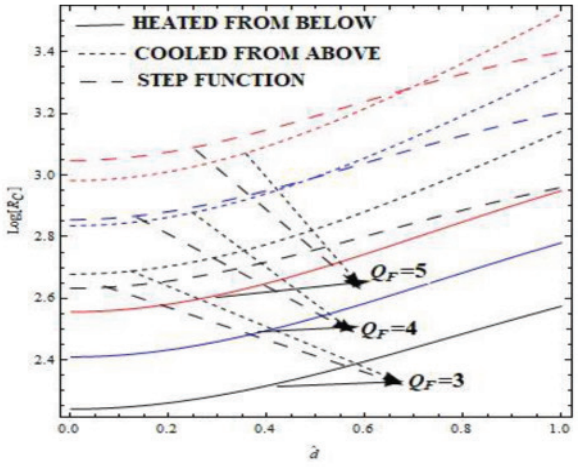

Figure 8.2

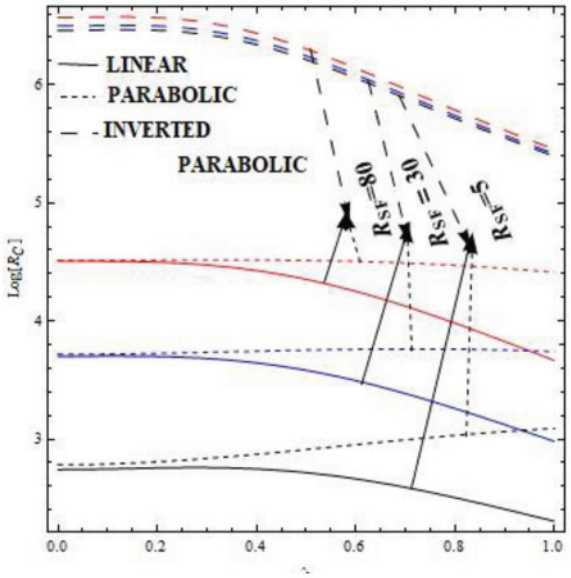

Figure 9.1

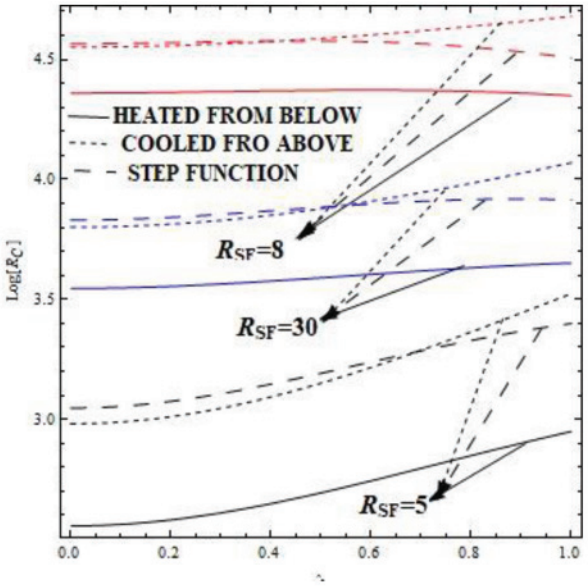

Figure 9.2

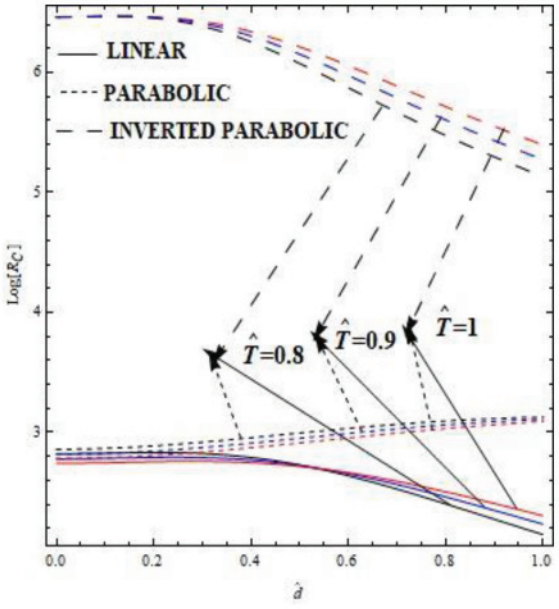

Figure 10.1

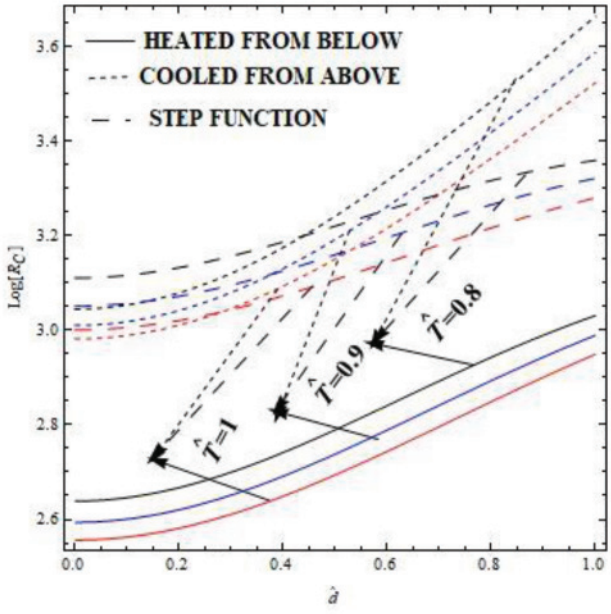

Figure 10.2

of PLHB profile and higher in case of PLCA profile.

The effects of ζ_f, fluid phase thermal expansion ratio on the critical Rayleigh number are shown in figures 4.1 and 4.2. It is seen that the curves are diverging with assigned values ζ_f = 1, 5 and 10 which proves that variation effect is protruding in case of two layer set up with $d_F \ll d_P$. It is also evident from the figure that increase in ζ_f results into decrease in critical Rayleigh number and hence the set-up can be destabilized. Smaller values of this parameter is appropriate in controlling of DDMDRB convection. Also, it is observed from the graph that inverted parablic profile is most stable whereas the linear profile is most unstable. Similarly, PLCA is most stable whereas PLHB is most unstable. The effect of the parameter is very less for parabolic profile and higher for inverted parabolic profile the whereas the effect of the parameter is very less in case of PLCA profile and higher in case of SF temperature profile.

The effects ofsolid phase thermal expansion ratio ζ_s over critical Rayleigh number are represented in figures 5.1 and 5.2 considering ζ_s = 2, 5 and 10. The

curves are found diverging showing that it is sensitive when the two layer set up is dominated by porous layer. Study reveals that the critical Rayleigh number decreases when ζ_s increases which destabilizes the system. Hence, there is quicker onset of DDMDRB convection. Lesser values of this parameter are preferable to control the same.

The effects of solid phase thermal diffusivity ratio $\hat{\kappa}_{sP}$ over critical Rayleigh number are depicted in figures 6.1 and 6.2 when $\hat{\kappa}_{sP}$ = 0.1, 0.5 and 1. Divergence is noticed from the figure and is evident that it is sensitive in two layer set up dominated by porous layer. Also, decrease in critical Rayleigh number is noticed when $\hat{\kappa}_{sP}$ increases which destabilizes the system. Hence, onset of DDMDRB convection is preponed. Smaller the values of this parameter, better the onset of convection is controlled.

The impact of inter-phase thermal diffusivity ratio τ over critical Rayleigh number are depicted in figures 7.1 and 7.2 for τ = 0.1, 0.5 and 1. The diverging curves indicate the sensitiveness of this parameter for the porous layer dominant two layer set up. The study reveals that the critical Rayleigh number decreases when t increases, thereby destabilizing the set-up. Hence onset of DDMDRB convection occurs quickly.

The effects of Chandrasekhar number Q_F over critical Rayleigh number are depicted in figures 8.1 and 8.2 when Q_F = 3, 4 and 5. The curves converge minutely and the observation using the graph is increase in critical Rayleigh number when Q_F increases with respect to all the six profiles. Hencethe set up gets stabilized thereby resulting in lateonset of DDMDRB convection.

The effects of solute Rayleigh number R_{SF} over critical Rayleigh number are depicted in figures 9.1 and 9.2. In this case, minute convergence of the curves is noticed when R_{SF} = 5, 30 and 80, indicating it is sensitive during dominance of porous layer over the two layer set up. Increase in critical Rayleigh number is observed when RSF increases. Hence the set-up is stable thereby delays the onset of DDMDRB convection. The effect of the parameter is very less for inverted parabolic profile and nertral in case of linear and parabolic profile the whereas the effect of the parameter is neutral with respect to PLHB, PLCA and SF temperature profile.

The effects of thermal ratio and 10.2 for the values of $\hat{T}$over critical Rayleigh number are represented in figures 10.1 $\hat{T}$ = 0.8, 0.9, 1. In this case the dual behaviour is observed. The effect of this parameter shows duality in case of linear profile. For $0 < \hat{d} < 0.5$, the set up gets destabilized and for $\hat{d} > 0.5$, it gets stabilized. Inverted parabolic profile shows postponement of the onset of DDMDRB convection and the profiles indicate earlier onset.

Conclusions

i. Porous parameter supports quicker onset of DDMDRB convection with respect to linear, parabolic, inverted parabolic, PLHB and PLCA profiles but delays the the onset for SF profile.
ii. In the fluid layer dominant two layer set up, linear profile is stable compared to PLHB whereas in porous layer dominant set up PLHB leads the role of stability.
iii. Similarly, in porous layer dominant two layer set up, PLCA is most stable whereas inverted parabolic profile is most unstable.
iv. With regard to all the six profiles, Chandrasekhar number and solute Rayleigh number stabilize the system thereby postpone the onset of DDMDRB convection.
v. Lower values of fluid phase and solid phase thermal expansion ratio, solid phase thermal diffusivity ratio and inter-phase diffusivity ratio are appropriate in controlling the onset of DDMDRB convection.
vi. With respect to Linear Profile, thermal ratio boosts the onset of DDMDRB convection in fluid layer dominant two layer set up whereas the onset of convection gets delayed in the porous layer dominant set up.
vii. Under the effect of thermal ratio, the onset of DDMDRB convection gets delayed in case of inverted parabolic profile and gets boosted for parabolic, PLHB, PLCA and SF temperature profile.

References

[1] Altawallbeh A.A. I. Hashim and A.A. Tawalbeh, Thermal Non-equilibrium Double Diffusive Convection in a Maxwell Fluid with Internal Heat Source, 3rd International Conference on Mathematical Sciences and Statistics, IOP Conf. Series: Journal of Physics: Conf. Series 1132 (2018) 012027, doi:10.1088/1742-6596/1132/1/012027.

[2] Atul Srivastava, B. S. Bhadauria Inûuence of Magnetic Field on Fingering Instability in a Porous Medium with Cross Diffusion Effect: a Thermal Non-equilibrium Approach, Journal of Applied Fluid Mechanics 9(6):2845-2853,

DOI:10.29252/jafm.09.06.25977.

[3] Daniel D. Joseph, Global stability of the conduction-diffusion solution, Archive for Rational Mechanics and Analysis volume 36, pages 285–292 (1970).

[4] Herbert E. Huppert, R. Stephen J. Sparks, Double-Diffusive Convection Due To Crystallization In Magmas, Ann. Rev. Earth Planet. Sci. 1984. 12.' 11-37.

[5] Ghazi Abed Meften, Ali Hasan Ali, Khalil S. Al-Ghafri, Jan Awrejcewicz and Omar Bazighifan, Nonlinear Stability and Linear Instability of Double-Diffusive Convection in a Rotating with LTNE Effects and Symmetric Properties: Brinkmann-Forchheimer Model, Symmetry 2022, 14(3), 565. https://doi.org/10.3390/sym1403056.

[6] Manjunatha N and Sumithra R, Effects of non-uniform temperature gradients on surface tension driven two component magneto convection in a porousfluid system, National Conference on Mathematical Techniques and its Applications (NCMTA 18), IOP Conf. Series: Journal of Physics: Conf. Series 1000 (2018) 012128 doi :10.1088/1742-6596/1000/1/012128

[7] Manjunatha N , Sumithra R, Vanishree R K, Combined effects of nonuniform temperature gradients and heat source on double diffusive Benard-Marangoni convection in a porous-fluid system in the presence of vertical magnetic field, International Journal of Thermofluid Science and Technology (2021) Volume 8, Issue 1, Paper No. 080104 https://doi.org/10.36963/IJTST.2021080104

[8] Mulone G, On the nonlinear stability of a fluid layer of a mixture heated and salted from below, Continuum Mech. Thermodyn. 6 (1994) 161-184.

[9] Pulkit Kumar Nadian , Rimple Pundir, Sudhir Kumar Pundir, Study Of Double- Diffusive Convection In A Rotating Couplestress Ferromagnetic Fluid In The Presence Of Varying Gravitational Field And Horizontal Magnetic Field Saturating In A Porous Medium, J. Math. Comput. Sci. 11 (2021), No. 2, 1784-1809 https://doi.org/10.28919/jmcs/5433 ISSN: 1927-5307.

[10] Rudraiah N, M.S. Malashetty, The Influence of Coupled Molecular Diffusion on DoubleDiffusive Convection in a Porous Medium, J. Heat Transfer. Nov 1986, 108(4): 872- 876, https://doi.org/10.1115/1.3247026

[11] Safia Akram, Maria Athar, Khalid Saeed, TaseerMuhammad and Mir Yasir Umair, Partial Slip Impact on Double Diffusive Convection Flow of Magneto-Carreau Nanofluid through Inclined Peristaltic Asymmetric Channel, Hindawi Mathematical Problems in Engineering Volume 2021, Article ID 2475846, 14 pages https://doi.org/10.1155/2021/2475846

[12] Xiaoli Qiang, Imran Siddique, Kashif Sadiq, Nehad Ali Shah, Double diffusive MHD convective flows of a viscous fluid under influence of the inclined magnetic field, source/sink and chemical reaction, Alexandria Engineering Journal, Volume 59, Issue 6, December 2020, Pages 4171-4181